Quaternary Science Reviews 224 (2019) 105973

Contents lists available at ScienceDirect

Quaternary Science Reviews

journal homepage: www.elsevier.com/locate/quascirev

Postglacial paleoceanography of the western Barents Sea: Implications for alkenone-based sea surface temperatures and primary productivity

Magdalena Łącka [a, *], Min Cao [b, c], Antoni Rosell-Melé [c, d], Joanna Pawłowska [a], Małgorzata Kucharska [a], Matthias Forwick [e], Marek Zajączkowski [a]

[a] Institute of Oceanology, Polish Academy of Sciences, Powstańców Warszawy 55, 81-712, Sopot, Poland
[b] Key Laboratory of Karst Environment, School of Geographical Sciences, Southwest University, Chongqing, 400715, China
[c] Institute of Environmental Science and Technology (ICTA-UAB), Universitat Autònoma de Barcelona, 08193, Bellaterra, Spain
[d] Institució Catalana de Recerca i Estudis Avançats, 08010 Barcelona, Spain
[e] Department of Geosciences, UiT The Arctic University of Norway in Tromsø, N-9037, Tromsø, Norway

ARTICLE INFO

Article history:
Received 12 February 2019
Received in revised form
26 September 2019
Accepted 29 September 2019
Available online xxx

Keywords:
Alkenones
Stratification
Holocene
Sea ice decrease
Global warming
North Atlantic Current
Arctic

ABSTRACT

The increasing influence of Atlantic Water (AW) in the Barents Sea, a process known as "Atlantification", is gradually decreasing sea ice cover in the region. Ongoing global climate warming is likely to be one of its drivers, but to further understand the role of natural variability and the biogeochemical impacts of the inflow of AW into the western Barents Sea, we reconstructed sea surface temperatures (SSTs) and primary productivity in Storfjordrenna, a climatically sensitive area south of Spitsbergen, between approximately 13,950 cal yr BP and 1300 cal yr BP. The alkenone $U^{K'}_{37}$ proxy has been applied to reconstruct SSTs, and the alkenone accumulation rate in marine sediments has been used to infer changes in primary productivity. Our data show that the SST increase was concomitant with the progressive loss of sea ice cover and an increase in primary productivity in the western Barents Sea. We interpret these changes as reflecting the increasing influence of AW in the area as the ice sheets retreated in Svalbard. The transition from the Arctic to the Atlantic domain first occurred after 11,500 cal yr BP, as the Arctic Front moved eastward of the study site but with considerable variability in surface ocean conditions. High SSTs at approximately 6400 cal yr BP may have led to limited winter surface cooling, likely inhibiting convective mixing and the return of nutrients to the euphotic zone and/or enhanced organic matter consumption by zooplankton due to an earlier light signal in the ice-free Storfjordrenna. During the late Holocene (3600-1300 cal yr BP), low insolation facilitated sea ice formation and thus brine production. The former may have launched convective water mixing and increased nutrient resupply to the sea surface, consequently enhancing primary productivity in Storfjordrenna. We propose that, on the basis of the paleoceanographic evidence, the modern increasing inflow of warm AW and the disappearance of pack ice on the Eurasian continental shelf are likely to weaken convective water mixing and decrease primary production in the region.

1. Introduction

The effects of ongoing climate warming are especially perceptible in the Arctic, mainly due to the rapid decline in the extent of sea ice over the past few decades, which numerous climate models expect to continue throughout the twenty-first century (e.g., Ding et al., 2017). The most striking changes in the extent and thickness of sea ice have occurred in the western Barents Sea (Onarheim et al., 2015; Yang et al., 2016). Sea ice decrease in the area is a reflection of the growing influence of Atlantic water (AW), a process sometimes referred to as "Atlantification" (e.g., Årthun et al., 2012; Oziel et al., 2016), which has caused the Barents Sea to reach its highest temperatures over the last decade, since systematic instrumental measurements began (Boitsov et al., 2012).

The accelerated loss of sea ice in the Barents Sea has a profound impact on the global energy budget, atmospheric and oceanic

* Corresponding author.
E-mail address: mlacka@iopan.gda.pl (M. Łącka).

https://doi.org/10.1016/j.quascirev.2019.105973

circulation, and the carbon cycle (Polyakov et al., 2017; Serreze and Barry, 2011). Among the Arctic shelf seas, the Barents Sea seafloor is the largest carbon sink, playing a significant role in controlling global atmospheric CO_2 concentrations and global climate (Smedsrud et al., 2013). Further decreases in ice cover and increases in surface water temperature in the western Barents Sea may cause primary productivity to decrease by 15–25% due to reduced nutrient flux into the upper ocean, resulting from decreasing advective mixing (Lewandowska et al., 2014; Lind et al., 2018). As the Barents Sea ecosystem supports some of the world's largest stocks of fish (Dalpadado et al., 2012, 2014), this issue also has global economic importance. In addition, more organic matter could be buried, relatively speaking, in the seasonally ice-covered northern Arctic regions than in the ice-free areas of the western Barents Sea (Pathirana et al., 2014; Slagstad et al., 2011).

The "Atlantification" of the western Barents Sea is a process that has occurred in the recent geological past. After the Younger Dryas (YD), the inflow of AW to the western Barents Sea (Hald et al., 2007; Ślubowska-Woldengen et al., 2008) and maximum Holocene summer insolation (Berger and Loutre, 1991) caused the increase in sea surface temperatures (SSTs) and decrease in sea ice (Rasmussen et al., 2014). Sea ice-free conditions remained during most of the mid-Holocene as a result of the influence of AW (Łącka et al., 2015b). These conditions coincided with the highest Holocene primary productivity observed on the northern continental slope of the Barents Sea (Wollenburg et al., 2004).

The objective of this study is to reconstruct the impact of AW inflow to the western Barents Sea, and its influence on primary productivity, from c. 13,950 cal yr BP to c. 1300 cal yr BP. We based our reconstruction on the alkenone $U^{K'}_{37}$ proxy to reconstruct SSTs (Bendle and Rosell-Melé, 2004) and the alkenone accumulation rate in marine sediments to infer the changes in primary productivity (e.g., Bolton et al., 2010). We compared our data to other studies conducted in the western Barents Sea continental slope (Martrat et al., 2003), the southwestern Barents Sea (Risebrobakken et al., 2010) and the Norwegian Sea (Calvo et al., 2002, Fig. 1; Table 1). The comparison provides new information on lateral and vertical oceanographic gradients, i.e., ocean vertical mixing, thermal stratification, and Arctic front movement in the western Barents Sea since the last deglaciation.

2. Oceanographic setting

The Barents Sea is an Arctic shelf sea located along the main pathway of heat and salt transport within the North Atlantic Current (NAC) entering the Arctic (Smedsrud et al., 2013; Rudels et al., 2015, Fig. 1). Thus, it is influenced by two main water masses, warm and saline AW and colder and fresher Arctic Water (ArW). AW ($T > 3\,^{\circ}C$, $S > 35.0$; Loeng, 1991) is transported northwards by the NAC, following the continental slope of Norway (Fig. 1A). The topographically steered flow of NAC bifurcates into two branches c. 72°N (Fig. 1A). One branch flows into the southern Barents Sea (i.e., North Cape Current), whereas the other branch continues northwards along the western Barents Sea slope and western Svalbard margin into the Arctic Ocean as the West Spitsbergen Current (Aagaard et al., 1987) (Fig. 1). The ArW ($T < 0\,^{\circ}C$, $S < 34.4$), formed by mixing of AW and polar waters in the Arctic Ocean, enters the Barents Sea from the north and is carried southward by the East Spitsbergen Current (ESC) (Loeng, 1991). At the boundary between Arctic and Atlantic water, a sharp gradient in terms of temperature, salinity, and sea-ice distribution is formed called the Arctic Front (AF; Hopkins, 1991). The AF determines the position of the marginal ice zone and surface productivity in the summer season (Smith and Sakshaug, 1990). At present, the AF is located east of our study area; however, the frontal zone changes its position, and water mixes and exchanges across the front (Walczowski, 2013; Łącka et al., 2015b).

The study area is the glacial trough of Storfjordrenna, located south of Spitsbergen (Fig. 1B). Storfjordrenna extends towards the north into Storfjorden, which is located north of a sill of 120 m depth. AW flows into Storfjordrenna in a cyclonic manner parallel to the trough's southern margin and along the northern slope towards its mouth (Fer et al., 2003). ArW enters the trough from the southeast with the ESC (Loeng, 1991). The uppermost 500 m of the water column at the mouth of Storfjordrenna contains relatively warm (4–7 °C) and saline (35.2) AW (Fig. 2A). Cold (−0.5 °C) intermediate water, generated by convection in the Nordic seas, occurs beneath the AW (Nilsen et al., 2008).

In the central part of Storfjordrenna, AW occurs between 50 and 160-m water depth (Fig. 2B). However, it is cooler here (max. 4.2 °C) than in the outer part of the Spitsbergen shelf (Fig. 2A). The surface water (SW) reaches 3.8 °C, which is comparable to the temperature of the AW at the Storfjordrenna mouth. However, it has a lower salinity (33.5; Fig. 2B) than the AW at the Storfjordrenna mouth. During the winter-freezing period, which typically lasts from late November to mid-May, brine-enriched shelf water (BSW) is produced in Storfjorden (Haarpaintner et al., 2001; Skogseth et al., 2004). BSW fills Storfjorden to the top of the sill and then begins a gravity-driven overflow through Storfjordrenna, further down the continental slope (Schauer et al., 2003). Thus, in Storfjordrenna, a 30-m-thick layer of BSW (temperature of approximately 0 °C and salinity slightly over 35.1) usually occurs in the deepest region immediately above the seafloor (Fig. 2B).

Northeast from Storfjordrenna, in the northern Barents Sea, AW flows via the Franz-Victoria Trough and the Kvitøya Trough, from the Eurasian continental slope (Fig. 1; Pfirman et al., 1994; Lind and Ingvaldsen, 2012) below the sea surface dominated by ArW (Gammelsrød et al., 2009). ArW occupies the upper 20–100 m of the northern Barents Sea, with temperature down to the freezing point (Lind and Ingvaldsen, 2012), whereas AW is found at depths of 150–350 m, has a salinity of 34.7 and a temperature of 1.1–0.8 °C (Fig. 2C) (Klitgaard-Kristensen et al., 2013). The northern Barents Sea experiences seasonal sea ice cover that forms during fall/winter (Loeng, 1991). Sea ice breakup occurs during summer, leading to open-water conditions in August and September (Belt et al., 2015). Recently, there is observed a decline in sea-ice formation in the northern Barents Sea, due to decrease in sea-ice import through the passage between Franz Josef Land and Novaya Zemlya, and a corresponding loss in freshwater, leading to weakened ocean stratification, enhanced vertical mixing and increased upward fluxes of heat and salt (Lind et al., 2018).

3. Materials and methods

3.1. Sediment cores

A 4.25-m-long gravity core JM09-020-GC (76.31489° N, 19.69957° E) was retrieved from a 253-m water depth in Storfjordrenna, with the R/V Jan Mayen (now: Helmer Hanssen; UiT The Arctic University of Norway) in November 2009 (Fig. 1). The coring site is located inside Storfjordrenna in a 3-km broad flat plain (<1% inclination); its location was selected after an echo-acoustic investigation in an area whose sediments were not under direct influence of brine-enriched waters. Conductivity-temperature-depth (CTD) measurements were performed in August 2015 at the coring site (Figs. 1 and 2).

The new results from core JM09-020-GC were compared to previously published alkenone data (Table 1). Core PSh-5159N (Risebrobakken et al., 2010) was retrieved from the SW Barents Sea (Fig. 1) at a water depth of 422 m. Its basal age is c. 15,000 cal yr BP. Core M23258-2 (Martrat et al., 2003) was recovered from the

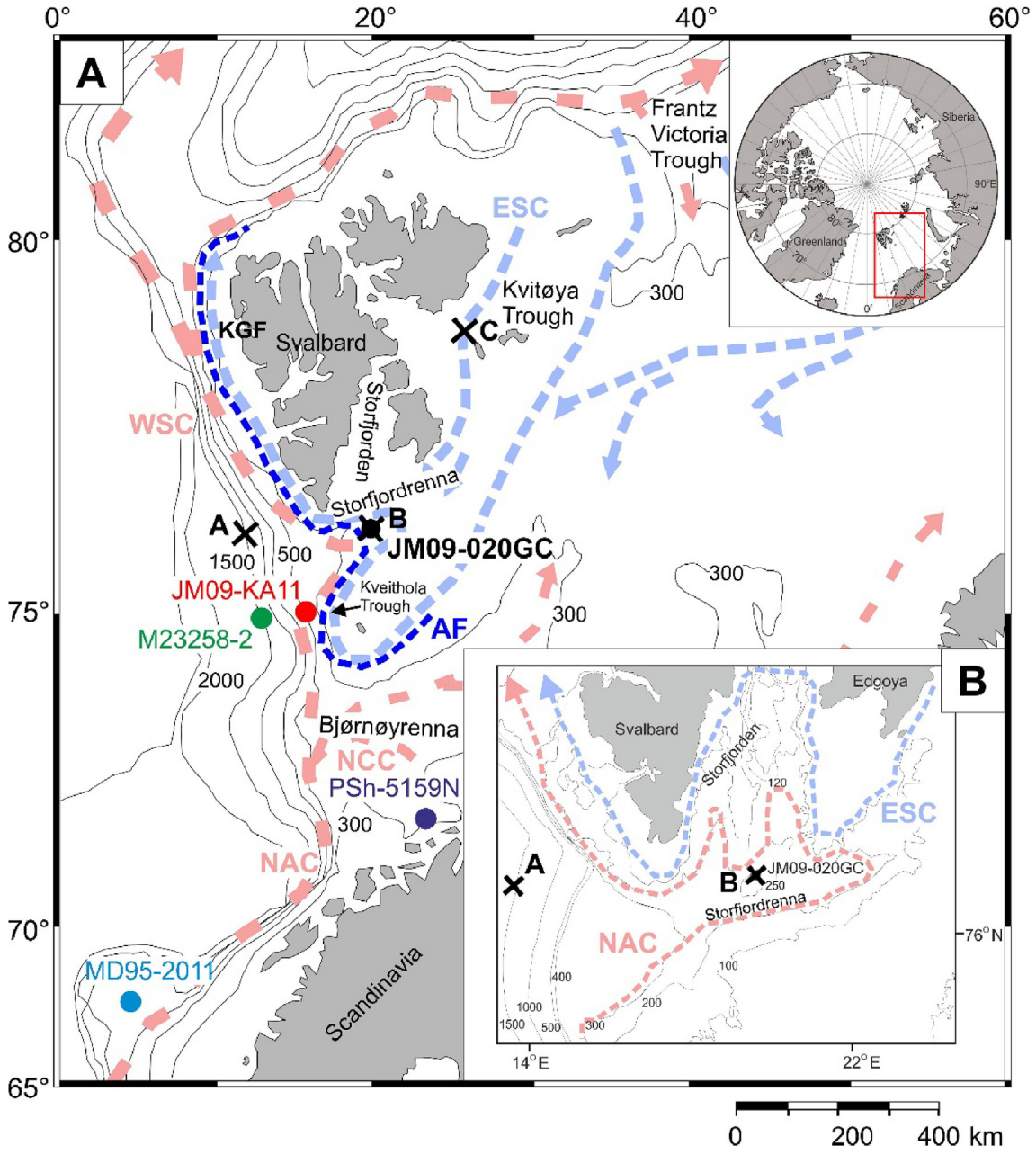

Fig. 1. Simplified map showing place names and core locations mentioned in the text, the dominant present-day surface water circulation in the Nordic and Barents Seas. The location of the studied core JM09-020 and the locations of the cores discussed in this paper are marked with dots: MD95-2011 (Calvo et al., 2002), PSh-5159N (Risebrobakken et al., 2010), M23258-2 (Martrat et al., 2003), and JM09-KA11 (Belt et al., 2015). Conductivity-temperature-depth (CTD) stations (A, B, and C) are marked with a black X. Red arrows represent Atlantic Water (AW), blue arrows represent Arctic Water (ArW), and royal blue dashed lines represent the Arctic Front (AF). The remaining abbreviations are as follows: NAC - North Atlantic Current, NCC- North Cape Current, WSC - West Spitsbergen Current, and ESC - East Spitsbergen Current. (For interpretation of the references to color in this figure legend, the reader is referred to the Web version of this article.)

Table 1
Positions of the cores and references to the original publications discussed in this paper.

Core	Location	Reference	Latitude (N)	Longitude (E)	Water depth (m)
JM09-020-GC	Storfjordrenna	This study	76.31°	19.70°	253
MD95-2011	NE Norwegian Sea	Calvo et al. (2002)	66.97°	7.63°	1048
PSh-5159N	SW Barents Sea	Risebrobakken et al. (2010)	71.36°	22.65°	422
M23258	W Barents Sea	Martrat et al. (2003)	74.99°	13.97°	1768

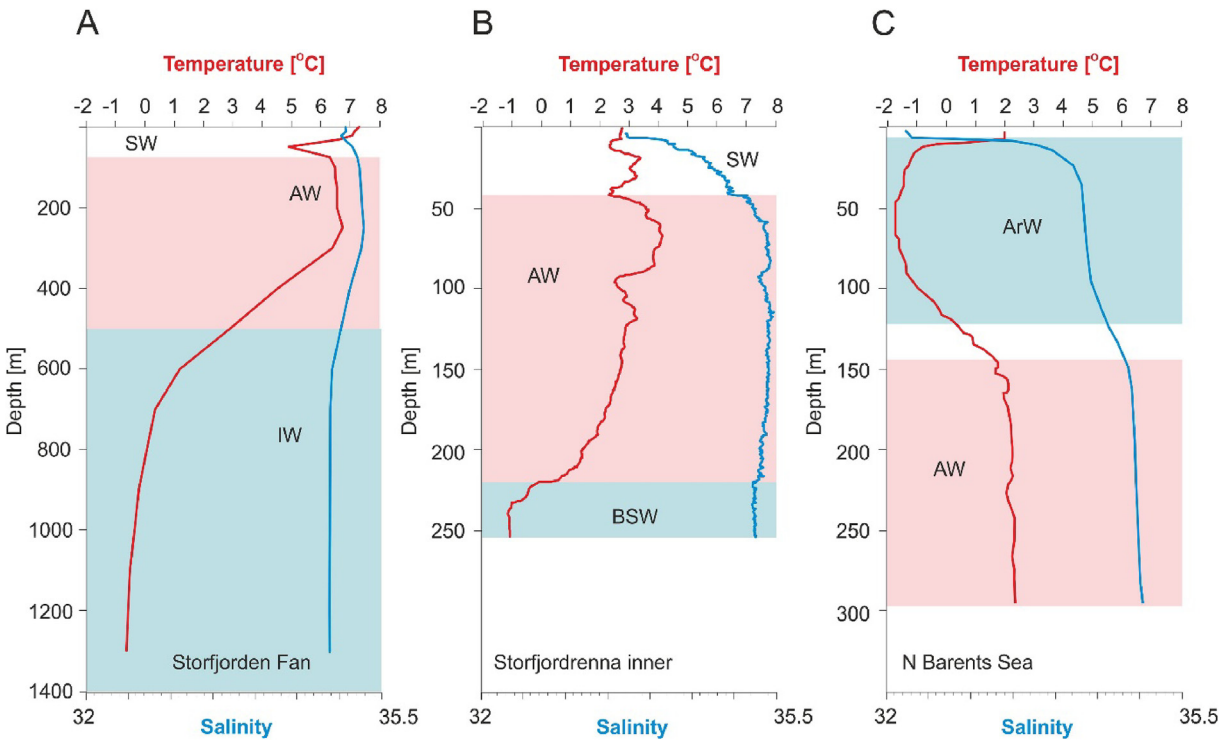

Fig. 2. Temperature and salinity profiles from A) the continental slope at the mouth of Storfjordrenna measured in August 2012 (1300-m water depth) (selected from the World Ocean Database https://www.nodc.noaa.gov/OC5/SELECT/dbsearch/dbsearch.html); B) Storfjordrenna (JM09-020 GC) measured in August 2015 at the inner part of the trough (253-m water depth; this study); C) the Kvitøya Trough (NP05-49) measured in August 2005 (300-m water depth) (Klitgaard-Kristensen et al., 2013). The colors on the conductivity-temperature-depth (CTD) profiles indicate the prevailing water masses. Abbreviations: SW - surface water, AW - Atlantic Water, ArW- Arctic Water, IW - intermediate water, and BSW - brine-enriched shelf water. The locations of the CTD stations are indicated in Fig. 1. (For interpretation of the references to color in this figure legend, the reader is referred to the Web version of this article.)

Barents Sea continental slope (Fig. 1) at a depth of 1768 m, and it spans over 15,000 cal yr BP. Core MD 95-2011 was collected in the eastern Norwegian Sea at a water depth of 1048 m (Fig. 1) and was dated to c. 13,800 cal yr BP (Calvo et al., 2002).

3.2. Chronology

A lithological description and a chronology of core JM09-020-GC were published by Łącka et al. (2015b). The AMS ^{14}C dates were converted into calibrated ages using the Marine13 calibration curve (Reimer et al., 2013) and a ΔR 105 ± 24 (Mangerud et al., 2006) in the calibration program Calib 7.1 (Stuiver and Reimer, 1993). The basal age of the sediment core was 13,950 cal yr BP. The lithological and micropaleontological investigation of the sediment core revealed that the core apparently represents continuous sedimentation, with no signs of redeposition and/or lateral sediment transport. The uppermost c. 40 cm of sediments were lost during coring; therefore, the age model for the sediment surface is cut off at 1300 cal yr BP (Łącka et al., 2015b). The time resolution of the record was between 10 and 400 years, depending on the core depth with the lowest resolution identified during the mid-Holocene (Supplement 1). The previously published age models for cores MD95-2011, PSh-5159N and M23258 have been recalibrated using Marine13 radiocarbon calibration curve (Reimer et al., 2013) in Calib 7.1 (Stuiver and Reimer, 1993).

3.3. Alkenone analysis

The alkenone analysis methodology is consistent with the standard methodology developed by Bendle and Rosell-Melé (2004). Individual subsamples for biomarker analysis collected at 1-5 cm intervals were ultrasonically extracted with dichloromethane/methanol (DCM/MeOH 3:1, v/v). An internal standard (2-nonadecanone, $C_{19}H_{38}O$, 3.5 ng/μL) was added to each test tube prior to the extraction of the biomarkers. The samples were extracted three more times using the same procedure, combined and treated with acid-activated copper to remove elemental sulfur. The total extracts were cleaned with open-column chromatography using hexane:DCM (1:1, v/v; 6 mL) and 6 mL of DCM (alkenone fraction).

Long-chain alkenones were quantified on an Agilent 7890A gas chromatograph with a flame ionization detector (GC-FID). The compounds were eluted through an Agilent HP-1 capillary column with a length of 60 m, an internal diameter of 0.25 mm, and a film thickness of 0.25 μm. External standards were used to identify the alkenones in the GC-FID based on their retention time. The quantification of alkenones was assessed using known concentrations of internal standards added prior to extraction. A solvent blank and sediment standard from Fram Strait (Rueda, 2013) were extracted with each batch of samples and analyzed in the same way as the rest of the samples. This routine allowed for the control of possible contamination during the preparative analysis of the samples and helped to recognize the alkenone peaks.

Alkenones are used widely to calculate the U^K_{37} indices in the North Atlantic region (Łącka et al., 2015a and references therein). The degree of alkenone unsaturation (the number of double bonds between the carbon atoms) provides an established way to reconstruct past ocean conditions (Brassell et al., 1986; Herbert, 2001; Marlowe et al., 1984; Volkman et al., 1980). However, according to Rosell-Mele (1998), when the $\%C_{37:4}$ value constitutes more than 5% of the total $\%C_{37}$ alkenone value and U^K_{37} is negative, the calculated temperatures are unreliable. In the case of JM09020-

GC, the values generally exceeded 5%. An alternative index to estimate SSTs for samples when $C_{37:4}$ values are significantly high was proposed by Bendle and Rosell-Melé (2004) as follows:

$$U_{37}^{K^*} = \frac{C_{37:2}}{C_{37:2} + C_{37:3} + C_{37:4}}$$

SSTs can be reconstructed using the alkenone-derived $U_{37}^{K^*}$ index (Bendle and Rosell-Melé, 2004) according to the following equation by Müller et al. (1998):

$$T(^{\circ}C) = \frac{U_{37}^{K^*} - 0.044}{0.033}$$

The statistical error of the regression is 1.5 °C. According to Müller et al. (1998) and Conte et al. (2006), the global core-top calibration of alkenone-based SST revealed that the best fit is obtained with annual mean SSTs. The same relationship was also established for polar and frontal regions (e.g., Müller and Fischer, 2004). In the study area, alkenone producers can bloom in summer, as well as in autumn when stratification of the upper water column breaks down, i.e., the sedimentary signal would potentially integrate a wider range of temperatures than just those from the warmest season.

To facilitate the comparison of our results with the published alkenone SST records in Calvo et al. (2002) and Martrat et al. (2003), we have recalculated the U_{37}^{K}-based SSTs according to the Bendle and Rosell-Melé (2004) $U_{37}^{K^*}$ model. The SST data after Risebrobakken et al. (2010) are presented in the original form, as the raw data are unavailable.

The total abundance of $C_{37:4}$ alkenones in the record was used as a tracer to infer variations in the water mass type as follows (Bendle et al., 2005):

$$\%C_{37:4} = \frac{C_{37:4}}{C_{37:2} + C_{37:3} + C_{37:4}} x100$$

In the subpolar and polar regions of the Nordic Seas, there is an increased proportion of the $C_{37:4}$ alkenone relative to the $C_{37:3}$ and $C_{37:2}$ alkenones (Rosell-Melé et al., 1994, Rosell-Mele, 1998). High $\%C_{37:4}$ values are associated with ArW, whereas low values are related to AW (Bendle et al., 2005). Hence, $\%C_{37:4}$ can also be used as an indicator of the AF position in the Nordic Seas (Rosell-Mele et al., 1998).

The absolute quantification of alkenones ($C_{37:2}$+$C_{37:3}$+$C_{37:4}$) was assessed using known concentrations of internal standards added prior to extraction and expressed as ΣC_{37} ng g^{-1} of dry sediment. The estimated level of detection was 3 ng g^{-1}, using an average sediment sample of 1 g dry weight. Concentration versus depth profiles can be potentially misleading with respect to quantitative interpretation of alkenone data, since they do not adequately reflect the influences of any changes in bulk sediment properties or accumulation rates. Therefore, alkenone concentrations were converted to annual fluxes, by combining individual sediment concentrations with sediment densities and accumulation rates derived from dry bulk density data and age/depth models, respectively.

4. Results

The SSTs in the lowermost part of the core (13,950–12,800 cal yr BP) varied between 0.5 °C and 5.5 °C (Fig. 3B). Both the alkenone flux and concentration (ΣC_{37}) were low (0.3–1.4 ng cm^{-2} a^{-1} and 7-32 ng g^{-1} sed, respectively; Fig. 3D), with a high contribution of $C_{37:4}$ (between 13% and 79%; Fig. 3A).

At approximately 12,800 cal yr BP, the alkenone concentrations dropped below the detection limit (Fig. 3D). Thus, SST estimates are missing. At approximately 12,600 cal yr BP, Storfjordrenna was covered by cold (T < 1 °C) surface water (Fig. 3B) with a high contribution of $C_{37:4}$ (c. 58%). Between 12,500 cal yr BP and 11,700 cal yr BP, the SSTs were slightly higher (average 2 °C; Fig. 3B), and the alkenone flux remained low (average 0.3 ng cm^{-2} a^{-1}; Fig. 3D). After 11,700 cal yr BP, the alkenone flux increased (up to 4 ng cm^{-2} a^{-1}; Fig. 3D) with a simultaneous decrease in $\%C_{37:4}$ (Fig. 3A).

A distinct decrease in $\%C_{37:4}$ (from 50% to approximately 25%; Fig. 3A) occurred c. 11,500 cal yr BP. This decrease was followed by a substantial SST increase, from an average of 2 °C to an average of 8.4 °C; however, SST oscillated significantly from 3 °C to 12.5 °C (Fig. 3B). At the same time, the alkenone flux remained relatively high (average 1.6 ng cm^{-2} a^{-1}; Fig. 3D).

Between 9200 cal yr BP and 3400 cal yr BP, SSTs in Storfjordrenna remained highly variable (from 3 °C to almost 13 °C; Fig. 3B). The $\%C_{37:4}$ varied between 7% and 38% (Fig. 3A), and the alkenone flux was very low (between 0.08 and 0.61 ng cm^{-2} a^{-1}).

After 3400 cal yr BP, the SSTs in Storfjordrenna ranged between 0.2 °C and 10 °C (Fig. 3B), with a rapid, concomitant increase in the alkenone flux (from 0.5 to 3 ng cm^{-2} a^{-1}). Towards the upper part of the core, the alkenone flux increased even more, reaching 12 ng cm^{-2} a^{-1} c. 1500 cal yr BP (Fig. 3D). At the same time, the $\%C_{37:4}$ varied between 9% and 25%; (Fig. 3A).

5. Discussion

5.1. Bølling-Allerød (13,950–12,800 cal yr BP)

Grounded ice retreated from Storfjordrenna during the B-A warming, c. 13,950 cal yr BP (Łącka et al., 2015b), as a consequence of the overall warming caused by the increase in the northern hemisphere insolation (Berger and Loutre, 1991). The SSTs at the study site during the B-A varied between 2 °C and 4 °C (Fig. 3B), which is comparable to modern SST values in Storfjordrenna (Fig. 2B). The modern-like conditions have also been noted on the Barents Sea continental slope, where SST reached 11 °C during the B-A (Martrat et al., 2003, Fig. 4A), which is comparable to the modern summer SST in this region (Trudnowska et al., 2016). Furthermore, the low $P_{III}IP_{25}$ (sea ice proxy) in the Kveithola Trough, south of Storfjordrenna (see the location of the JM09-KA11 core in Fig. 1), indicate stable ice edge or marginal ice zone conditions at that time (Fig. 4D) (Belt et al., 2015). The sea ice conditions in Storfjordrenna during the B-A could be driven by prevailing southwesterly winds. The modern sea ice occurrence in Storfjordrenna arises from seasonal ice advected from the Arctic Ocean and the Barents Sea (Hendricks et al., 2011) and is strictly connected to the prevailing wind direction. According to Skogseth et al. (2004), the amount of sea ice in the western Barents Sea is high during winters dominated by northeasterly winds and when temperatures are low, whereas in winters dominated by southwesterly winds, the inflow of the AW increases SSTs, and the sea ice decreases.

Although the B-A SSTs were comparable to contemporary values, the alkenone concentration and flux at the study site were low (Fig. 3D), with a high contribution of $C_{37:4}$ (between 13% and 79%; Fig. 3A). This inverse relationship between ΣC_{37} and $C_{37:4}$ indicates that fewer alkenones were produced in the fresher ArW. High $\%C_{37:4}$ values have been found in modern surface sediments in regions where surface temperatures and salinity are both low (Bendle and Rosell-Melè, 2004; Bendle et al., 2005; Harada et al., 2006), e.g., high $\%C_{37:4}$ values (up to 70%) have been noted in the waters of the East Greenland Current, where the sea ice cover reached approximately 80% (Bendle et al., 2005). Phytoplankton productivity is much lower in these ArWs than in AWs (Andreassen

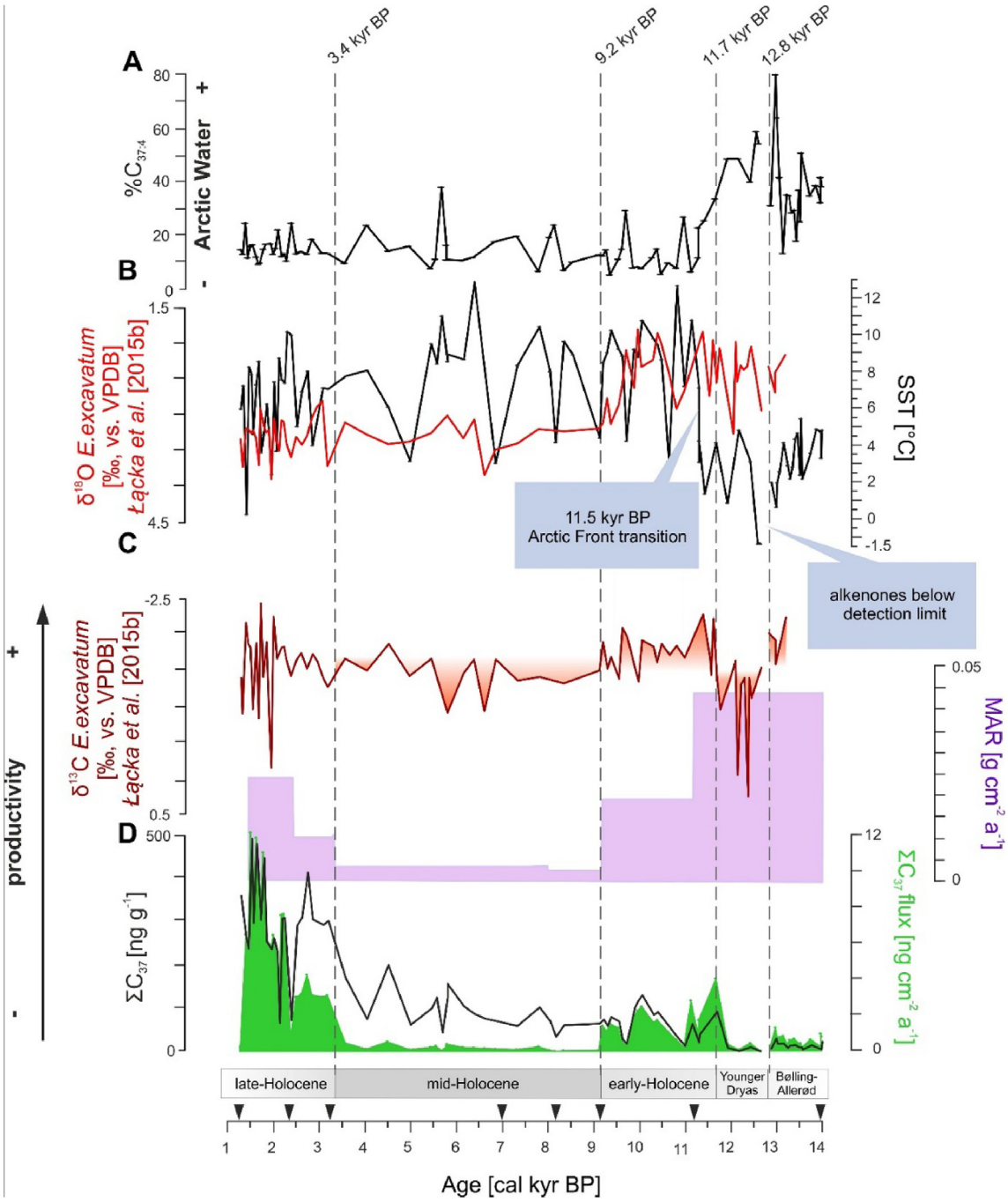

Fig. 3. Proxy records from core JM09-020 GC A) $\%C_{37:4}$; B) U^{K*}_{37}-based sea surface temperatures (SSTs; right scale) and stable oxygen isotope data (red line; left scale; Łącka et al., 2015b); C) stable carbon isotope data (burgundy line; left scale; Łącka et al., 2015b) and mass accumulation rates (g cm^{-2} a^{-1}; violet shading; right scale; Łącka et al., 2015b); D) total alkenone concentrations (ΣC37; ng g^{-1}; black line; left scale) and total alkenone flux (ng cm^{-2} a^{-1}; green shading; right scale). The black triangles on the x axis denote the AMS ^{14}C converted to calibrated radiocarbon ages (after Łącka et al., 2015b). The Arctic Front transition at 11,500 cal yr BP is marked. (For interpretation of the references to color in this figure legend, the reader is referred to the Web version of this article.)

et al., 1996). However, the low concentration of alkenones could also result from their degradation and/or dilution by the high sediment supply (e.g., Hoefs et al., 1998). A high sediment accumulation rate in Storfjordrenna (43 g $cm^{-2}kyr^{-1}$) during this interval (Fig. 3C; Łącka et al., 2015b) supports the latter interpretation.

Much lower alkenone concentrations during the B-A were also noted on the Barents Sea continental slope (Martrat et al., 2003), indicating that the AF was located further to the west than it is today. This difference was caused by the proximity of the retreating Svalbard Barents Sea Ice Sheet (SBSIS) front, which was located in the inner basin of Storfjorden at that time (e.g., Rasmussen and Thomsen, 2014) and released large amounts of turbid meltwater (Łącka et al., 2015b), limiting primary productivity (Fig. 4C). This process is observed today in glaciated fjords on Svalbard, where, despite relatively high SSTs, productivity remains low (Kubiszyn et al., 2014; Piwosz et al., 2009; Zajączkowski, 2008). We conclude that the oceanographic conditions in Storfjordrenna

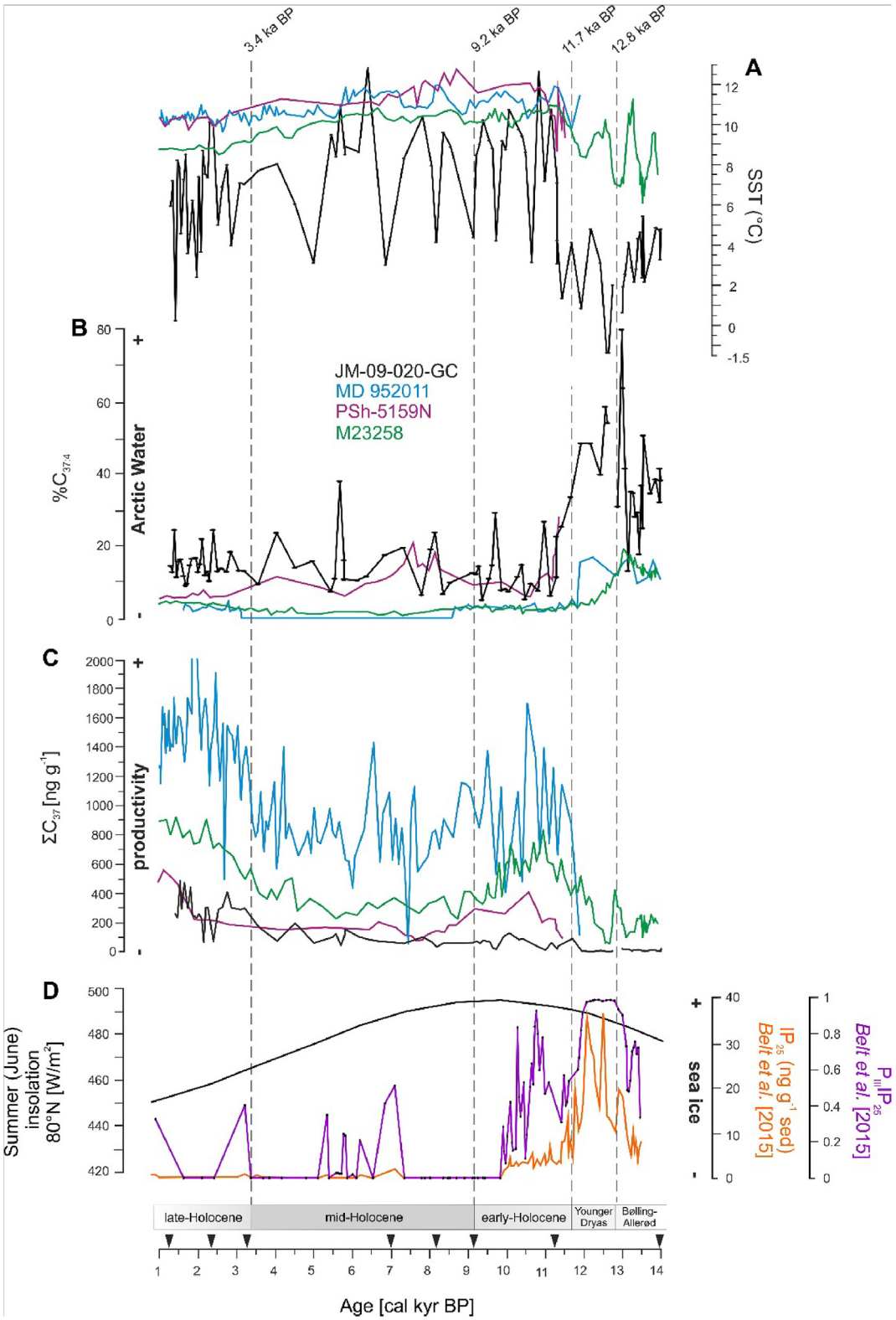

Fig. 4. Comparison of A) $U^{K's}_{37}$-based sea surface temperatures (SSTs; right scale); B) $\%C_{37:4}$; C) total alkenone concentrations (ΣC37; ng g^{-1}) from the current study (JM09-020 GC; black line), western Barents Sea (Martrat et al., 2003) (M23258; green line), the southwestern Barents Sea (Risebrobakken et al., 2010) (PSh-5159N; purple line), and the northeastern Norwegian Sea (Calvo et al., 2002) (MD95-2011; blue line); and D) summer insolation (June) at 80° N (Berger and Loutre, 1991; black line, left scale) and IP_{25} (orange line, right scale), and $P_{III}IP_{25}$ (purple line, right scale) records from the core JM09-KA11 obtained from the western Barents Sea (after Belt et al., 2015) showing the sea ice conditions. The black triangles on the x axis denote the AMS ^{14}C converted to calibrated radiocarbon ages (after Łącka et al., 2015b). (For interpretation of the references to color in this figure legend, the reader is referred to the Web version of this article.)

during the B-A were similar to modern conditions in the innermost parts of the glaciated fjords of western Svalbard.

5.2. Younger Dryas (12,800–11,700 cal yr BP)

The onset of the YD (12,800 cal yr BP) in Storfjordrenna was characterized by low alkenone concentrations, occasionally remaining below the detection limit (Fig. 3D). This extremely low alkenone signal indicates a reduction in primary productivity that persisted for several decades. Similarly, low or absent primary production is observed beneath modern pack ice in the Arctic Ocean (Antoniades et al., 2011; Darby et al., 2006), suggesting that sea ice covered the area. Another explanation for the low or lack of alkenone signal might be postdepositional degradation. However, Łącka et al. (2015b) noticed, based on the absence of ice-rafted debris in this interval, that the beginning of YD in Storfjordrenna was characterized by temporary polar conditions and the formation of perennial pack ice in Storfjorden that locked icebergs proximal to their calving fronts, thus preventing their movement over the coring site. Therefore, we suggest that Storfjordrenna was covered by perennial sea ice at the onset of the YD, limiting light penetration into the surface water and subsequently restricting phytoplankton growth.

At c. 12,600 cal yr BP, Storfjordrenna was covered by cold ($T < 1\,^{\circ}C$) surface water (Fig. 3B) of Arctic origin, as seen from the high values of $\%C_{37:4}$ (Fig. 3A). The surface productivity at the study site increased slightly (Fig. 3D). However, Łącka et al. (2015b) noted a lighter $\delta^{18}O$ signal from benthic foraminifera, indicating the presence of warmer waters at the bottom (Fig. 3B). The nearly continuous presence of warmer and more saline AW during the beginning of the YD was also noted in the subsurface waters of the southern Nordic Seas by Knudsen et al. (2004) and Rasmussen et al. (2011). The difference between cold, less saline surface water and warmer but high saline bottom water indicates stratification, which was essential for the presence of sea ice, since the pycnocline protected the cold sea surface from the heat stored in the AW below. According to Rasmussen et al. (2014), the pycnocline over the western Spitsbergen shelf occurred at depths between 100 m and 150 m at this time, because of the freshwater supply from the decaying SBSIS. Our data may indicate that the oceanographic conditions of Storfjordrenna at this time were similar to modern conditions in the northern Barents Sea (Fig. 1), with strong water column stratification, prolonged seasonal sea ice cover (Fig. 2C) and lower marine productivity (Fig. 3D). However, as the lighter $\delta^{18}O$ can also point to the changes in bottom water salinity, more studies are needed to confirm our hypothesis. Nevertheless, the severe seasonal sea ice cover throughout the YD also occurred 150 km south of our coring site, in the Kveithola Trough, as indicated by high $P_{III}IP_{25}$ values (Belt et al., 2015) (Fig. 4D). Further west, the continental margin remained ice free; however, the SST decreased to 7 °C, and the alkenone production also decreased significantly (Martrat et al., 2003, Fig. 4C).

Between 12,500 cal yr BP and 11,700 cal yr BP, the SST in Storfjordrenna increased (average 2 °C); however, surface productivity remained low (Fig. 3B and D). This might have resulted from the continuous delivery of turbid waters from the decaying SBSIS (Łącka et al., 2015b), which strongly limited light penetration and consequently led to decreased primary productivity and/or alkenone signal dilution (compare with Hoefs et al., 1998). At the same time, the mineral particles in the surface waters absorbed an amount of sunlight energy (e.g., Kara et al., 2005) that was close to the maximum Holocene values (Fig. 4D), thereby elevating the SST in Storfjordrenna. A widespread hypothesis regarding the mechanism of the YD cold spell suggests that the YD cooling resulted from a slowdown in the AMOC (e.g., Ritz et al. (2013) and references therein). Nevertheless, AW influenced numerous locations in the North Atlantic region throughout the YD (Bartels et al., 2017; Łącka et al., 2015b; Pearce et al., 2013; Rasmussen et al., 2007), leading to variable sea ice conditions in the Nordic Seas during the latter part of YD (Bakke et al., 2009; Cabedo-Sanz et al., 2013). Our data indicate that heavy sea ice conditions prevailed in Storfjordrenna only at the very beginning of the YD. In the later part of YD, the oceanography of Storfjordrenna was modified by interactions between Arctic and Atlantic waters, as indicated by the variability in SST (Fig. 3B) and $\%C_{37:4}$ (Fig. 3A). The similar pattern in alkenone record has been also observed on the continental slope of the Barents Sea, where after 12,200 cal yr BP ArW contribution decreased concomitant with the productivity increase (Fig. 4 B and C). Contradictory, the $P_{III}IP_{25}$ signal from Kveithola Trough pointed to the continuous presence of consistently long seasonal sea ice cover (Belt et al., 2015).

5.3. Early Holocene (11,700-9200 cal yr BP)

At the beginning of the early Holocene (11,700 cal yr BP), the alkenone concentrations in Storfjordrenna increased and the $\%C_{37:4}$ decreased, indicating the increasing influence of AW in the trough, a reduction in sea ice, as well as an increase in marine productivity (Fig. 3C). A similar oceanographic change was noted in the southwestern Barents Sea by Risebrobakken et al. (2010) and in the Norwegian Sea by Calvo et al. (2002). In the record after Martrat et al. (2003), further decrease in $\%C_{37:4}$ and increase in productivity was observed. The transition from prolonged seasonal ice cover to ice-edge conditions is also supported by the $P_{III}IP_{25}$ signal from the western Barents Sea, which indicates that sea ice cover at that time was variable (Belt et al., 2015).

Approximately 11,500 cal yr BP, a rapid transition from an Arctic to an Atlantic water-dominated environment occurred in Storfjordrenna, suggesting that AF passed our study site and moved eastward. This is illustrated by a further decrease in $\%C_{37:4}$ (from 50% to approximately 25%; Fig. 3A) and a substantial SST increase, from an average of 2 °C prevailing during the YD to 3–12.5 °C at the beginning of the Holocene (Fig. 3B). Today, such high SSTs (average 8.4 °C; Fig. 3B) are observed in the core of the West Spitsbergen Current flowing west of Spitsbergen (e.g., Trudnowska et al., 2016); however, they are less variable than the SSTs during the early Holocene. A significant increase of SSTs shows AW appearance in the upper part of the water column. However, the high amplitudes in SST prevailing throughout the entire Holocene indicate the continuous proximity of the AF to our study site (Fig. 3B). The SST variability presented in Fig. 3B corresponds to the pulsatory inflow of ArW shown in Fig. 3A. The location of the AF closer to the Spitsbergen coast at approximately 11,500 cal yr BP is also confirmed by the increase in productivity in Storfjordrenna (higher alkenone flux and lighter $\delta^{13}C$; Fig. 3C and D). The presence of a highly productive frontal zone at our study site is also visible in the higher abundance of the AF proximity proxy, i.e., the benthic foraminifera *Nonionellina labradorica,* in Storfjordrenna (Łącka et al., 2015b). The timing of the AF transition in Storfjordrenna was the same as that on the Barents Sea continental slope (Martrat et al., 2003) and that farther south in the eastern Norwegian Sea (Calvo et al., 2002) (Fig. 4B), where $\%C_{37:4}$ decreased to modern values characteristic of the AW domain, i.e., 5% (Rosell-Mele et al., 1998). Previously, Łącka et al. (2015b) based on $\delta^{18}O$ concluded that the transition from the Arctic to the Atlantic domain occurred at approximately 9600 cal yr BP (Fig. 3B), because the lighter $\delta^{18}O$ is characterized for the ArW of Barents Sea origin (Duplessy et al., 2005). Indeed, the $\delta^{18}O$ values are still shifted towards the lighter values, but this could be also caused by the continuous production of brine in Storfjordrenna. Although the AW dominated at the

surface, sea ice formed during the polar night, and lower $\delta^{18}O$ brine was delivered to the bottom of Storfjordrenna (Fig. 3B).

Early Holocene SSTs in Storfjordrenna were variable and reached the Holocene temperature maximum (Fig. 3B). Because the alkenone record is susceptible to temperature changes related to orbital forcing (Risebrobakken et al., 2011), we suggest that the SST changes observed during the early Holocene in Storfjordrenna and on the adjacent continental shelf resulted from both AW inflow and a peak in the northern hemisphere summer insolation (Berger and Loutre, 1991) (Fig. 4D). The presence of warm AW was found in the early Holocene at the northern tip of Svalbard (Bartels et al., 2017) and even farther in the northwestern Barents Sea (Ivanova et al., 2019). The appearance of AW at the sea surface in Storfjordrenna suggests that the contribution of turbid meltwater diminished, as confirmed by the reduced sediment accumulation rate at the core site during the early Holocene (Fig. 3C; Łącka et al., 2015b). Indeed, according to Forwick and Vorren (2009) and Hughes et al. (2016), after the YD-early Holocene transition, the final deglaciation of Svalbard and Scandinavia occurred, and after 10,000 cal yr BP, the glaciers in western Svalbard were even smaller than those of the present day.

5.4. Mid-Holocene (9200-3400 cal yr BP)

SSTs in Storfjordrenna varied significantly during the mid-Holocene (Fig. 3B), although in the western Barents Sea continental margin (Martrat et al., 2003) and in the Norwegian Sea (Calvo et al., 2002) they remained stable (10 °C and 11.5 °C, respectively) (Fig. 4A). Over the European continental slope, warm AW dominated at the surface during this period, as confirmed by the absence or low values of $C_{37:4}$ alkenone (Fig. 4B; Calvo et al., 2002; Martrat et al., 2003). Conversely, high $\%C_{37:4}$ (10-20%) values were found in Storfjordrenna sediments (Fig. 3A; this study) and in the southwestern Barents Sea (Risebrobakken et al., 2010), which could suggest a continuous ArW contribution (Fig. 4B) at those sites. A feasible explanation of the SST variability on the western shelf of the Barents Sea could be the alternating influence of the ESC with the NAC.

At approximately 6400 cal yr BP, the SST in Storfjordrenna reached a peak of almost 13 °C (Fig. 3B) and the $\%C_{37:4}$ decreased (Fig. 3A), indicating significant AW inflow. Based on benthic foraminifera assemblages, especially the occurrence of *Melonis barleeanum*, Łącka et al. (2015b) suggested that around that time, the Storfjordrenna sea environment was similar to that of the contemporary Norwegian fjords, which are dominated by AW with temperatures of 6–8 °C. Our new alkenone data confirm this finding. Additionally, the finding is supported by the occurrence of *Mytilus edulis* on the western and eastern coasts of Svalbard at this time (Salvigsen, 2002; Mangerud and Svendsen, 2018), as *M. edulis* is a thermophilous mollusk spawning at temperatures above 8-10 °C (Thorarinsdóttir and Gunnarsson, 2003). The mid-Holocene is often referred to as the Holocene Thermal Maximum (HTM) in marine and terrestrial records (Risebrobakken et al., 2011). The high SST predominated throughout the European Arctic, reducing sea ice formation up to the northern margins of the Svalbard shelf (Müller et al., 2012) and in the central Arctic Ocean (Polyak et al., 2010). However, the SST maximum occurred when the summer insolation had already started to decrease, after a maximum peak during the early Holocene (Berger and Loutre, 1991, Fig. 4D). This indicates that, at this time, the main heat source was the enhanced inflow of AW, and insolation played a secondary role in the heating of Storfjordrenna surface waters.

During the mid-Holocene, the alkenone flux in Storfjordrenna was very low (Fig. 3D). In the other records discussed here, the alkenone concentration also decreased, which suggests low sea surface productivity in the Norwegian and Svalbard shelf areas (Fig. 4C). The low productivity in the region is also confirmed by high $\delta^{13}C$ and the low benthic foraminifera flux in Storfjordrenna (Fig. 3C) (Łącka et al., 2015b), as well as low benthic foraminifera flux further south, in Kveithola Trough (Groot et al., 2014). Two basic factors regulate primary productivity in the ocean: sunlight and nutrient availability. During the polar day, insolation is high, but light penetration throughout the water column can be limited by water turbidity. According to Łącka et al. (2015b), the sediment flux was low (approximately 0.019–0.002 g cm^{-2} yr^{-1}; Fig. 3C) in Storfjordrenna during the mid-Holocene because of the reduced glaciers on Svalbard. Therefore, we suggest that the most important factor limiting primary productivity in the study area was nutrient availability. According to Behrenfeld et al. (2006), reduced nutrient flux into the upper oceans can be caused by enhanced thermal vertical stratification. The high SST in Storfjordrenna that prevailed approximately 6400 cal yr BP (Fig. 3A) most likely limited the surface cooling during the winter and consequently inhibited convective water mixing and the return of nutrients to the euphotic zone. Wollenburg et al. (2004) found that productivity increased in the northern Barents Sea (at latitude 81°N) during the mid-Holocene. The mid-Holocene productivity maximum (seen as maximum planktic and benthic foraminifera abundances) was also noted by Ślubowska et al. (2005) in a sediment core obtained from the northern Svalbard continental margin at 80°N. Thus, we suggest that the high productivity zone at that time shifted northward to the region where Arctic pack ice appeared seasonally, causing sea surface cooling in winter and inducing convective water mixing. Our suggestion is supported by the northward and eastward shift of the ice edge and phytoplankton blooms in the modern Barents Sea observed over the last 17 years (Oziel et al., 2017).

An alternative explanation of the low primary productivity in Storfjordrenna could be the earlier light signal in the spring in the ice-free water and the earlier appearance of mesozooplanktonic organisms in the sea surface. According to Zajączkowski et al. (2010), in the ice-free Adventfjorden (western Spitsbergen), the open-water spring period enhanced primary productivity. However, the majority of the particulate organic matter was then consumed by zooplankton, and the organic matter sedimentation was much lower in this period than in the ice-covered years. Additional investigations are needed to verify these two scenarios.

5.5. Late Holocene (3400-1300 cal yr BP)

After 3400 cal yr BP, the SSTs in Storfjordrenna decreased and ranged from 10 °C to approximately 0 °C (Fig. 3A). Total alkenone flux increased rapidly (Fig. 3D). Throughout the entire late Holocene, further gradual surface water cooling occurred, reflecting increases in alkenone flux. A similar alkenone signal pattern was detected in both the southwestern Barents Sea (Risebrobakken et al., 2010) and the Norwegian Sea (Calvo et al., 2002) (Fig. 4A and C). In general, this cooling trend corresponded to further decreases in northern hemisphere insolation (Fig. 4D; Berger and Loutre, 1991). We suggest that the cooler surface of Storfjordrenna froze periodically at that time and produced brine, which launched convective water mixing and increased nutrient resupply to the sea surface. Consequently, primary production was enhanced in the area, as is supported by other productivity proxies such as higher benthic foraminifera flux (Łącka et al., 2015b). Simultaneously, diminished surface water productivity was noted in the inner Storfjorden, stemming from dense, packed sea ice cover (Knies et al., 2017). South of Storfjordrenna, in the Kveithola Trough, $P_{III}IP_{25}$ was mainly absent throughout the late Holocene, reflecting the predominantly ice-free ocean conditions (Belt et al., 2015) (Fig. 4D). According to Risebrobakken and Berben (2018),

the AF in Kveithola Trough was shifted towards inner part of the trough at that time. We suggest that the difference in the location of the AF was caused by other local environmental conditions.

Late Holocene near-bottom conditions in Storfjordrenna were characterized by variable oceanographic conditions and higher salinity and temperature gradients because of the proximity of the AF that resulted from the reduced inflow of AW (Łącka et al., 2015b). This finding is supported by our new data on SSTs and other alkenone records published by Calvo et al. (2002) and Martrat et al. (2003) (Fig. 4A). SSTs decreased (c. 1-2 °C), and marine productivity increased. Moreover, an increased $\%C_{37:4}$ (Fig. 3A) indicates a greater contribution of ArW, suggesting continuous sea ice formation inducing the convective replenishing of nutrients from the bottom to the surface.

6. Summary and conclusions

Alkenone analyses in sediment core JM-09-020GC from Storfjordrenna were performed with the purpose of reconstructing SSTs, the relative influences of AW and ArW, the location of the AF, as well as the marine primary productivity in the western Barents Sea between approximately 13,950 cal yr BP and 1300 cal yr BP. The proposed sequence of climatic and oceanographic events in the time period studied are as follows:

The SSTs in Storfjordrenna during the B-A warming were comparable to modern SST values. They were probably the result of increased insolation and the reinvigoration of the AMOC. However, we argue that the constant delivery of turbid meltwater from the Svalbard glaciers caused a significant decrease in marine productivity, unlike the present day situation in the core site location.

At the onset of the YD (12,800 cal yr BP), Storfjordrenna was covered by perennial sea ice, causing light limitations in the surface water and a subsequent reduction in phytoplankton growth. At approximately 12,600 cal yr BP, Storfjordrenna was covered by cold surface water, which we proposed caused water column stratification and was essential for sea ice formation. Thus, a marked pycnocline could have isolated the cold sea surface from the heat stored in the AW below. After 12,500 cal yr BP, the surface conditions in Storfjordrenna gradually ameliorated, and AW appeared at the surface, leading to a transition from the long seasonal ice cover to sea ice edge conditions. Although the YD is regarded as a stadial period, the present study shows that heavy sea ice conditions prevailed in Storfjordrenna only at the onset of the YD. In the middle part of the YD, the oceanography of Storfjordrenna was modified by interactions between Arctic and Atlantic waters, causing SST variability.

The early Holocene in Storfjordrenna (11,700–9200 cal yr BP) was characterized by a transition from an Arctic to an Atlantic domain. The alkenone records can be interpreted to show that at approximately 11,500 cal yr BP, the AF passed the study site and moved eastward. Early Holocene warming was driven by the increasing northern hemisphere insolation and final decay of the SBSIS, leading to a shift from ice-sheet proximal to ice-sheet distal conditions at the study site. The high SSTs between 6400 and 3400 cal yr BP maintained water stratification in winter as well as inhibited convective water mixing and the return of nutrients to the euphotic zone and/or enhanced organic matter consumption by zooplankton, due to earlier light signals in the ice-free Storfjordrenna. The high productivity zone at this time shifted from Storfjordrenna to the northern edge of the Eurasian shelf, where Arctic pack ice enabled sea surface cooling in winter and induced convective water mixing. During late the Holocene (3400-1300 cal yr BP), low insolation facilitated sea ice formation and brine production, which launched convective water mixing and increased nutrient resupply to the sea surface, consequently enhancing the primary productivity in Storfjordrenna.

Based on past changes in Arctic oceanography, combined with observations in the modern Barents Sea (e.g., Oziel et al., 2017), we suggest that the increasing inflow of warm AW and the disappearance of pack ice on the Eurasian continental shelf may weaken convective water mixing during the polar night and may limit spring/summer primary production in the region.

Acknowledgments

We acknowledge the National Science Centre in Poland for its financial support through project no. 2016/21/B/ST10/02308 (alkenone analysis) and 2012/05/N/ST10/03696 (other analyses) and the Spanish research Ministry Maria de Maeztu award MDM-2015-0552. We also extend our thanks to the captain and crew of the R/V Jan Mayen and the cruise participants, in particular Steinar Iversen, for their help at sea. Eva Calvo and Belen Martrat are gratefully acknowledged for providing their alkenone data. We are also very grateful to Agnieszka Promińska for data processing. We acknowledge two anonymous reviewers for their constructive comments on the manuscript.

Appendix A

Depth [cm]	Age BP	C37:4	C37:3	C37:2	%C37:4	UK37*	SST UK37* Muller
5	1290.71421	88.41	366.76	144.11	14.75270324	0.2404719	5.953693928
9	1332.42654	13.49	60.78	29.16	13.04263753	0.281929808	7.20999417
13	1401.94709	82.87	235.51	17.4	24.6798499	0.051819644	0.236958903
17	1457.56353	20.75	101.29	56.19	11.64226	0.31526679	8.220205761
21	1513.17997	99.95	340.12	190.77	15.84395409	0.302406315	7.830494406
25	1554.8923	82.34	317.44	96.96	16.57607602	0.195192656	4.58159564
29	1624.41285	88.28	441.85	210.32	11.92247957	0.284043487	7.274045063
33	1680.02929	9.87	61.69	34.47	9.308686221	0.325096671	8.518080932
37	1721.74162	39.06	295.7	65	9.770862518	0.162597559	3.59386541
41	1791.26217	100.87	443.2	130.81	14.94636083	0.193827051	4.540213659
45	1846.87861	62.17	217.28	92.86	16.69845022	0.249415809	6.224721497
53	1958.11149	44.84	188.21	32.79	16.86728859	0.123344869	2.404389973
57	2013.72793	53.22	238.87	118.52	12.96120406	0.288643725	7.413446218
61	2069.34437	55.28	247.76	59.69	15.23998566	0.16455766	3.653262423
65	2124.96081	26.49	53.8	39.8	22.05845616	0.331418103	8.709639488
69	2180.57725	47.97	230.31	115.14	12.1930761	0.292664328	7.535282673
73	2236.19369	55.93	246.19	121.68	13.19726286	0.287116564	7.367168619
77	2291.81013	6.02	29.57	21.68	10.51161166	0.378557709	10.1381124

(*continued*)

Depth [cm]	Age BP	C37:4	C37:3	C37:2	%C37:4	UK37*	SST UK37* Muller
81	2391.42853	33.15	51.14	50.15	24.65783993	0.37302886	9.970571529
85	2505.71425	51.79	258.85	81.99	13.19053562	0.208822556	4.994622897
89	2619.99997	71.56	300.61	138.88	14.00254378	0.271754231	6.901643378
93	2734.28569	46.66	198.48	109.15	13.17000198	0.308080951	8.00245305
97	2848.57141	79.58	274.74	75.11	18.53154181	0.174906271	3.9668567
105	3077.14285	60.72	266.53	126.31	13.38742394	0.278485757	7.105629004
109	3191.42857	64.84	286.15	133.91	13.37182924	0.276160033	7.035152515
113	3571.5625	24.37	152.48	75.53	9.656074174	0.299270941	7.73548305
117	4040.3125	31.59	59.93	41.02	23.83431417	0.309491474	8.04519619
121	4509.0625	23.52	102.36	40.52	14.13461538	0.243509615	6.045745921
125	4977.8125	14.75	64.03	13.61	15.96493127	0.147310315	3.130615605
129	5446.5625	9.56	70.14	44.27	7.711543115	0.357102525	9.487955297
130	5563.75	28.4	143.78	81.35	11.20183016	0.320869325	8.389979549
131	5680.9375	24.36	13.69	26.06	37.99719233	0.406488847	10.98451052
132	5798.125	33.54	104.93	66.67	16.34980989	0.324997563	8.515077656
133	5798.125	23.75	119.52	73.26	10.96845703	0.338336489	8.919287551
135	6149.6875	18.71	98.34	57.35	10.72821101	0.328841743	8.631567973
137	6384.0625	11.37	39.68	44.77	11.86599875	0.467230223	12.82515828
141	6852.8125	18.94	72.48	15.27	17.75236667	0.143124941	3.003786104
145	7327	19.09	46.88	30.85	19.71700062	0.318632514	8.322197392
149	7803	9.67	78.97	56.09	6.681406757	0.38754923	10.41058272
151	8041	24.16	62.69	38.5	19.27403271	0.307140008	7.973939636
152	8160	8.84	21.5	6.69	23.87253578	0.180664326	4.141343219
153	8352	7.71	61.89	39.34	7.077290252	0.361116211	9.609582144
154	8544	5.34	29.72	17.84	10.09451796	0.337240076	8.886062897
157	9120	13.62	72.37	20.01	12.8490566	0.188773585	4.38707833
161	9204.60732	13.53	60.1	35.16	12.43680485	0.32319147	8.46034757
165	9289.21464	17.33	60.67	40.34	14.64424539	0.340882204	8.996430419
169	9373.82196	4.9	51.96	35.1	5.328403654	0.38168769	10.23296031
177	9543.0366	11.8	56.78	36.61	11.21779637	0.348036886	9.213238959
181	9627.64392	3.55	12.28	7.97	14.91596639	0.33487395	8.814362108
185	9712.25124	8.77	15.63	5.46	29.37039518	0.182853315	4.207676226
193	9881.46588	16.87	121.05	73.36	7.9846649	0.347216963	9.188392826
197	9966.0732	10.33	72.89	41.59	8.276580402	0.333226504	8.764439524
201	10050.68052	16.04	108.87	82.82	7.721561643	0.398690608	10.74820024
213	10304.50248	22.87	100.44	71.16	11.76016866	0.365917622	9.755079462
217	10389.1098	27.37	89.79	64.48	15.0682669	0.354987888	9.423875398
221	10473.71712	4.78	53.62	28.55	5.497412306	0.328349626	8.61665534
229	10642.93176	10.49	80.52	15.78	9.823017136	0.147766645	3.144443782
237	10812.1464	4.73	27.75	27.78	7.849319615	0.461002323	12.63643404
245	10981.36104	8.2	13.72	8.59	26.87643396	0.281547034	7.198394962
256	11136.36364	5.917	48.63	36.19	6.521044337	0.398845014	10.7528792
273	11290.90909	5.29	27.6	12.7	11.6034218	0.278569862	7.108177631
274	11300	19.82	51.16	15.98	22.79208832	0.183762649	4.235231803
275	11425	3.32	8.56	1.15	25.47966232	0.088257866	1.341147469
277	11675	6.38	9.21	3.42	33.56128353	0.179905313	4.118342818
279	11925	11.61	10.64	1.72	48.43554443	0.071756362	0.841101882
281	12175	2.46	1.59	1.03	48.42519685	0.202755906	4.810785016
283	12425	6.64	7.61	2.44	39.78430198	0.146195327	3.096828077
285	12577.08333	3.27	2.32	0	58.49731664	0	−1.333333333
287	12631.25	2.96	2.52	0	54.01459854	0	−1.333333333
291	12739.58333						
292	12766.66667						
296	12875	4.67	8.75	1.64	31.00929615	0.108897742	1.966598253
300	12983.33333	47.05	8.14	3.82	79.73224877	0.064734791	0.628326991
301	13010.41667	22.03	8.86	3.75	63.59699769	0.108256351	1.947162153
303	13064.58333	20.88	22.95	6.44	41.53570718	0.128108216	2.548733807
306	13145.83333	7.23	37.2	9.75	13.34440753	0.179955703	4.119869794
309	13227.08333	8.3	12.06	3.29	35.09513742	0.139112051	2.882183356
311	13281.25	10.51	16.2	3.49	34.8013245	0.115562914	2.168573149
313	13335.41667	2.28	4.68	1.1	28.28784119	0.136476427	2.802315964
315	13389.58333	10	17.62	6.33	29.455081	0.186450663	4.31668675
317	13443.75	5.2	18.13	5.73	17.89401239	0.197178252	4.641765209
319	13497.91667	8.25	11.44	2.73	36.79750223	0.12176628	2.356553943
320	13525	2.93	6.16	2.61	25.04273504	0.223076923	5.426573427
321	13552.08333	6.92	5.18	1.58	50.58479532	0.115497076	2.166578061
328	13741.66667	12.35	17.53	5.74	34.67153285	0.161145424	3.549861331
333	13862.5	2.64	2.81	1.4	38.54014599	0.204379562	4.859986729
349	13966.07143	3.64	5.42	2.25	32.18390805	0.198938992	4.695120971
353	13973.21429	25.66	26.85	9.39	41.453958	0.151696284	3.263523768
361	13987.5	41.34	45.06	21.96	38.15060908	0.202657807	4.807812343

Appendix B

Depth [cm]	Age BP	Concentration [ng/g]				Flux
		C37:4	C37:3	C37:2	C37SUM	
5	1290.71421	53.04666856	220.0587734	86.75531339	359.8607554	0.399911
13	1401.94709	65.03106385	184.8131513	13.65440462	263.4986198	6.424431
17	1457.56353	27.87734803	136.081763	75.23887993	239.1979909	5.831951
21	1513.17997	77.77767941	264.6697781	147.9558687	490.4033262	11.95666
25	1554.8923	49.34041767	190.2188752	58.48846907	298.0477619	7.266783
29	1624.41285	57.05254478	285.5535445	135.9230994	478.5291887	11.66715
37	1721.74162	29.72679445	225.0438587	49.79834231	304.5689954	7.425779
41	1791.26217	66.72572082	293.1777483	86.53109488	446.434564	10.88464
45	1846.87861	42.43731238	148.315574	64.02020454	254.7730909	6.211692
53	1958.11149	40.03573422	168.0447265	29.17921096	237.2596717	5.784692
57	2013.72793	33.97158726	152.476382	75.90630523	262.3542745	6.396531
61	2069.34437	35.28689835	158.1527123	38.35594782	231.7955585	5.65147
65	2124.96081	15.01101939	30.48670605	22.4781846	67.97591004	1.657339
69	2180.57725	37.40676185	179.5945658	90.38415654	307.3854842	7.494449
73	2236.19369	40.80960124	179.6337516	88.78441406	309.2277669	7.539366
81	2391.42853	18.24908823	28.15259041	27.60759501	74.00927365	0.765834
85	2505.71425	38.52618225	192.556522	61.39834127	292.4810456	3.026539
89	2619.99997	43.44250786	182.4937435	84.02996795	309.9662193	3.207472
93	2734.28569	54.29214597	230.945245	127.4269401	412.6643311	4.270173
97	2848.57141	56.63742218	195.5336186	53.81247833	305.9835191	3.16626
105	3077.14285	39.27497179	172.3972041	81.4276287	293.0998046	3.032942
109	3191.42857	40.58523168	179.1095627	82.9799613	302.6747557	3.132021
113	3571.5625	16.59153093	103.8111053	51.25076475	171.653401	0.528979
117	4040.3125	18.40218485	34.91114081	24.05476438	77.36809004	0.238423
121	4509.0625	30.79533865	134.0225708	35.72294199	200.5408514	0.618
125	4977.8125	10.20589518	44.30396395	9.448490902	63.95835002	0.197098
129	5446.5625	7.884813505	57.84945808	36.39091613	102.1251877	0.314716
130	5563.75	14.18922277	71.8354384	40.77960975	126.8042709	0.390769
131	5680.9375	17.510013	9.840397289	18.6070963	45.95750659	0.141626
132	5798.125	20.88423652	65.33640245	41.78993428	128.0105733	0.394486
133	5798.125	17.31400309	87.13135364	53.58534508	158.0307018	0.486998
135	6149.6875	11.4440418	60.15003049	34.84448736	106.4385597	0.328008
137	6384.0625	12.47831699	43.54789957	32.91981958	88.94603614	0.274102
139	6618.4375	11.19929201	53.22689577	13.86206074	78.28824851	0.241258
141	6852.8125	12.94514574	49.53876259	10.5063459	72.99025423	0.224932
145	7327	12.12583424	29.77784752	19.66102285	61.56470461	0.199847
149	7803	6.97993157	57.00157147	40.48649036	104.4679934	0.339117
151	8041	13.85355565	35.94699518	22.29699964	72.09755048	0.158642
152	8160	8.842603666	21.50633245	6.736583558	37.08551967	0.081602
153	8352	4.528609886	36.35222644	23.03004685	63.91088317	0.140628
157	9120	8.599867886	45.6954801	12.46614623	66.76149421	0.1469
161	9204.60732	9.536243161	42.35980887	24.69894027	76.5949923	1.469983
165	9289.21464	9.052845678	31.69279557	21.07280985	61.8184511	1.186397
169	9373.82196	4.383258505	46.48043101	31.39844358	82.26213309	1.578744
177	9543.0366	7.996511123	38.47812725	24.97491136	71.44954974	1.371233
181	9627.64392	4.613664168	15.95937915	10.39252763	30.96557095	0.59428
185	9712.25124	6.117922304	10.90343508	3.82157377	20.84293115	0.40001
193	9881.46588	8.235218342	59.09147483	35.93061073	103.2573039	1.981676
197	9966.0732	9.854906876	69.53767301	39.94172451	119.3343044	2.29022
201	10050.68052	10.17330995	69.0503899	52.70336918	131.927069	2.531895
213	10304.50248	10.20487748	44.81757298	31.96415721	86.98660768	1.669415
217	10389.1098	14.18583956	46.53805386	33.19711054	93.92100396	1.802497
229	10642.93176	5.840208141	44.82874733	8.873219191	59.54217467	1.142711
237	10812.1464	2.973365047	17.44416069	17.34659911	37.76412485	0.724755
245	10981.36104	4.345921937	7.271469388	4.582969013	16.20036034	0.310911
256	11136.36364	5.00027305	41.09570364	20.49064065	66.58661733	2.83411
273	11290.90909	5.279225257	14.72625993	3.398749343	23.40423453	0.996149
274	11300	9.532718171	24.60614842	7.737052907	41.8759195	1.782354
277	11675	31.64814907	45.68643463	17.07809524	94.41267894	4.018463
279	11925	5.354861784	4.907470231	0.785379728	11.04771174	0.470221
281	12175	2.098636993	1.356436105	0.875768611	4.330841709	0.184333
283	12425	5.225739741	5.989138468	1.920301953	13.13518016	0.559069
285	12577.08333	3.173916974	2.251831003	0	5.425747976	0.230935
287	12631.25	1.753015669	1.492432259	0	3.245447928	0.138135
291	12739.58333					
292	12766.66667					
296	12875	3.132830539	5.8698645	1.092845782	10.09554082	0.429694
300	12983.33333	25.90820206	4.482311684	2.103492707	32.49400645	1.383034
301	13010.41667	12.98241677	5.22125341	2.209898452	20.41356864	0.868858

(*continued*)

Depth [cm]	Age BP	Concentration [ng/g]				Flux
		C37:4	C37:3	C37:2	C37SUM	
306	13145.83333	2.890517667	14.87237306	3.885007666	21.64789839	0.921394
309	13227.08333	4.026166618	5.850068604	1.595914238	11.47214946	0.488286
311	13281.25	5.815876481	8.964528924	1.905497317	16.68590272	0.710198
313	13335.41667	4.724536762	9.697733353	2.28697971	16.70924982	0.711192
315	13389.58333	5.361766013	9.447431714	3.393997886	18.20319561	0.774778
317	13443.75	2.581143775	8.999257045	2.84422189	14.42462271	0.613952
319	13497.91667	4.501449818	6.242010414	1.489570667	12.2330309	0.520671
320	13525	3.143706097	6.609293364	2.800366182	12.55336564	0.534306
321	13552.08333	3.693124811	2.764506722	0.851660198	7.309291731	0.311104
328	13741.66667	6.067274671	8.612091092	2.801132165	17.48049793	0.744018
349	13966.07143	2.647012014	3.941429977	1.647110498	8.235552488	0.350528
353	13973.21429	10.416686	10.89976691	3.862698776	25.17915169	1.071694
361	13987.5	7.943709193	8.658527727	4.233801001	20.83603792	0.886839

Appendix C. Supplementary data

Supplementary data to this article can be found online at https://doi.org/10.1016/j.quascirev.2019.105973.

References

Aagaard, K., Foldvik, A., Hillman, S.R., 1987. The West Spitsbergen Current: disposition and water mass transformation. J. Geophys. Res.: Oceans 92 (C4), 3778–3784.

Andreassen, I., Nöthig, E.-M., Wassmann, P., 1996. Vertical particle flux on the shelf off northern Spitsbergen, Norway. Mar. Ecol. Prog. Ser. 137, 215–228.

Antoniades, D., Francus, P., Pienitz, R., St-Onge, G., Vincent, W.F., 2011. Holocene dynamics of the Arctic's largest ice shelf. Proc. Natl. Acad. Sci. U. S. A. 108, 18899–18904.

Årthun, M., Eldevik, T., Smedsrud, L.H., Skagseth, Ø., Ingvaldsen, R., 2012. Quantifying the influence of Atlantic heat on Barents Sea ice variability and retreat. J. Clim. 25, 4736–4743.

Bakke, J., Lie, Ø., Heegaard, E., Dokken, T., Haug, G.H., Birks, H.H., Dulski, P., Nilsen, T., 2009. Rapid oceanic and atmospheric changes during the Younger Dryas cold period. Nat. Geosci. 2 (3), 202.

Bartels, M., Titschack, J., Fahl, K., Stein, R., Seidenkrantz, M.-S., Hillaire-Marcel, C., Hebbeln, D., 2017. Atlantic Water advection vs. glacier dynamics in northern Spitsbergen since early deglaciation. Clim. Past 13, 1717–1749.

Behrenfeld, M.J., O'Malley, R.T., Siegel, D.A., McClain, C.R., Sarmiento, J.L., Feldman, G.C., Boss, E.S., 2006. Climate-driven trends in contemporary ocean productivity. Nature 444, 752–755.

Belt, S.T., Cabedo-Sanz, P., Smik, L., Navarro-Rodriguez, A., Berben, S.M., Knies, J., Husum, K., 2015. Identification of paleo Arctic winter sea ice limits and the marginal ice zone: optimised biomarker-based reconstructions of late Quaternary Arctic sea ice. Earth Planet. Sci. Lett. 431, 127–139.

Bendle, J., Rosell-Melé, A., 2004. Distributions of $U^{K'}_{37}$UK37 and $U^{K'}_{37}$UK37′ in the surface waters and sediments of the Nordic Seas: implications for paleoceanography. Geochem. Geophys. Geosyst. 5 (11), Q11013.

Bendle, J., Rosell-Melé, A., Ziveri, P., 2005. Variability of unusual distributions of alkenones in the surface waters of the Nordic seas. Paleoceanography 20, PA2001.

Berger, A., Loutre, M.-F., 1991. Insolation values for the climate of the last 10 million years. Quat. Sci. Rev. 10, 297–317.

Boitsov, V.D., Karsakov, A.L., Trofimov, A.G., 2012. Atlantic water temperature and climate in the Barents Sea, 2000–2009. ICES J. Mar. Sci. 69, 833–840.

Bolton, C.T., Lawrence, K.T., Gibbs, S.J., Wilson, P.A., Cleaveland, L.C., Herbert, T.D., 2010. Glacial–interglacial productivity changes recorded by alkenones and microfossils in late Pliocene eastern equatorial Pacific and Atlantic upwelling zones. Earth Planet. Sci. Lett. 295, 401–411.

Brassell, S., Eglinton, G., Marlowe, I., Pflaumann, U., Sarnthein, M., 1986. Molecular stratigraphy: a new tool for climatic assessment. Nature 320, 129–133.

Cabedo-Sanz, P., Belt, S.T., Knies, J., Husum, K., 2013. Identification of contrasting seasonal sea ice conditions during the Younger Dryas. Quat. Sci. Rev. 79, 74–86.

Calvo, E., Grimalt, J., Jansen, E., 2002. High resolution U^{K}_{37}U 37 K sea surface temperature reconstruction in the Norwegian Sea during the Holocene. Quat. Sci. Rev. 21, 1385–1394.

Conte, M.H., Sicre, M.A., Rühlemann, C., Weber, J.C., Schulte, S., Schulz-Bull, D., Blanz, T., 2006. Global temperature calibration of the alkenone unsaturation index ($U^{K'}_{37}$UK' 37) in surface waters and comparison with surface sediments. Geochem. Geophys. Geosyst. 7 (2), 2006Q02005.

Dalpadado, P., Ingvaldsen, R.B., Stige, L.C., Bogstad, B., Knutsen, T., Ottersen, G., Ellertsen, B., 2012. Climate effects on Barents Sea ecosystem dynamics. ICES J. Mar. Sci. 69, 1303–1316.

Dalpadado, P., Arrigo, K.R., Hjøllo, S.S., Rey, F., Ingvaldsen, R.B., Sperfeld, E., Ottersen, G., 2014. Productivity in the Barents Sea-response to recent climate variability. PLoS One 9 (5), e95273.

Darby, D.A., Polyak, L., Bauch, H.A., 2006. Past glacial and interglacial conditions in the Arctic Ocean and marginal seas–a review. Prog. Oceanogr. 71, 129–144.

Ding, Q., Schweiger, A., L'Heureux, M., Battisti, D.S., Po-Chedley, S., Johnson, N.C., Blanchard-Wrigglesworth, E., Harnos, K., Zhang, Q., Eastman, R., 2017. Influence of high-latitude atmospheric circulation changes on summertime Arctic sea ice. Nat. Clim. Chang. 7, 289–295.

Duplessy, J.C., Cortijo, E., Ivanova, E., Khusid, T., Labeyrie, L., Levitan, M., Murdmaa, I., Paterne, M., 2005. Paleoceanography of the Barents Sea during the Holocene. Paleoceanography 20, PA4004.

Fer, I., Skogseth, R., Haugan, P.M., Jaccard, P., 2003. Observations of the Storfjorden overflow. Deep-Sea Res. Part I Oceanogr. 50, 1283–1303.

Forwick, M., Vorren, T.O., 2009. LateWeichselian and Holocene sedimentary environments and ice rafting in Isfjorden, Spitsbergen. Palaeogeogr. Palaeoclimatol. Palaeoecol. 280, 258–274.

Gammelsrød, T., Leikvin, Ø., Lien, V., Budgell, W.P., Loeng, H., Maslowski, W., 2009. Mass and heat transports in the NE Barents Sea: observations and models. J. Mar. Syst. 75, 56–69.

Groot, D.E., Aagaard-Sørensen, S., Husum, K., 2014. Reconstruction of Atlantic water variability during the Holocene in the western Barents Sea. Clim. Past 10 (1), 51–62.

Haarpaintner, J., Gascard, J.-C., Haugan, P.M., 2001. Ice production and brine formation in Storfjorden, Svalbard. J. Geophys. Res. 106, 013.

Hald, M., Andersson, C., Ebbesen, H., Jansen, E., Klitgaard-Kristensen, D., Risebrobakken, B., Salomonsen, G.R., Sarnthein, M., Sejrup, H.P., Telford, R.J., 2007. Variations in temperature and extent of Atlantic water in the northern North Atlantic during the Holocene. Quat. Sci. Rev. 26, 3423–3440.

Harada, N., Ahagon, N., Sakamoto, T., Uchida, M., Ikehara, M., Shibata, Y., 2006. Rapid fluctuation of alkenone temperature in the southwestern Okhotsk Sea during the past 120 ky. Glob. Planet. Chang. 53, 29–46.

Hendricks, S., Gerland, S., Smedsrud, L., Haas, C., Pfaffhuber, A., Nilsen, F., 2011. Sea-ice thickness variability in Storfjorden, Svalbard. Ann. Glaciol. 52, 61–68.

Herbert, T., 2001. Review of alkenone calibrations (culture, water column, and sediments). Geochem. Geophys. Geosyst. 2, 2000GC000055.

Hoefs, M.J., Versteegh, G.J., Rijpstra, W.I.C., de Leeuw, J.W., Damsté, J.S.S., 1998. Postdepositional oxic degradation of alkenones: implications for the measurement of palaeo sea surface temperatures. Paleoceanography 13 (1), 42–49.

Hopkins, T.S., 1991. The GIN Sea: a synthesis of its physical oceanography and literature review, 1972–1985. Earth Sci. Rev. 30, 175–318.

Hughes, A.L., Gyllencreutz, R., Lohne, Ø.S., Mangerud, J., Svendsen, J.I., 2016. The last Eurasian ice sheets–a chronological database and time-slice reconstruction. DATED-1. Boreas 45, 1–45.

Ivanova, E., Murdmaa, I., de Vernal, A., Risebrobakken, B., Peyve, A., Brice, C., Seitkalieva, E., Pisarev, S., 2019. Postglacial paleoceanography and paleoenvironments in the northwestern Barents Sea. Quat. Res. 1–20.

Kara, A.B., Wallcraft, A.J., Hurlburt, H.E., 2005. Sea surface temperature sensitivity to water turbidity from simulations of the turbid Black Sea using HYCOM. J. Phys. Oceanogr. 35 (1), 33–54.

Knies, J., Pathirana, I., Cabedo-Sanz, P., Banica, A., Fabian, K., Rasmussen, T.L., Forwick, M., Belt, S.T., 2017. Sea-ice dynamics in an Arctic coastal polynya during the past 6500 years. Arktos 3, 1.

Knudsen, K.L., Eiríksson, J., Jansen, E., Jiang, H., Rytter, F., Gudmundsdóttir, E.R., 2004. Palaeoceanographic changes off North Iceland through the last 1200 years: foraminifera, stable isotopes, diatoms and ice rafted debris. Quat. Sci. Rev. 23, 2231–2246.

Kristensen, D.K., Rasmussen, T.L., Koç, N., 2013. Palaeoceanographic changes in the northern Barents Sea during the last 16 000 years–new constraints on the last deglaciation of the Svalbard–Barents Sea ice sheet. Boreas 42, 798–813.

Kubiszyn, A., Piwosz, K., Wiktor Jr., J., Wiktor, J., 2014. The effect of inter-annual Atlantic water inflow variability on the planktonic protist community structure in the West Spitsbergen waters during the summer. J. Plankton Res. 36,

1190–1203.
Lewandowska, A.M., Boyce, D.G., Hofmann, M., Matthiessen, B., Sommer, U., Worm, B., 2014. Effects of sea surface warming on marine plankton. Ecol. Lett. 17, 614–623.
Lind, S., Ingvaldsen, R.B., 2012. Variability and impacts of Atlantic water entering the Barents Sea from the North. Deep-Sea Res. Part I Oceanogr. 62, 70–88.
Lind, S., Ingvaldsen, R.B., Furevik, T., 2018. Arctic warming hotspot in the northern Barents Sea linked to declining sea-ice import. Nat. Clim. Chang. 8, 634–639.
Loeng, H., 1991. Features of the physical oceanographic conditions of the Barents Sea. Polar Res. 10, 5–18.
Mangerud, J., Bondevik, S., Gulliksen, S., Hufthammer, A.K., Høisæter, T., 2006. Marine 14C reservoir ages for 19th century whales and molluscs from the North Atlantic. Quat. Sci. Rev. 25, 3228–3245.
Mangerud, J., Svendsen, J.I., 2018. The Holocene thermal maximum around Svalbard, Arctic North Atlantic; molluscs show early and exceptional warmth. Holocene 28 (1), 65–83.
Marlowe, I., Brassell, S., Eglinton, G., Green, J., 1984. Long chain unsaturated ketones and esters in living algae and marine sediments. Org. Geochem. 6, 135–141.
Martrat, B., Grimalt, J.O., Villanueva, J., van Kreveld, S., Sarnthein, M., 2003. Climatic dependence of the organic matter contributions in the north eastern Norwegian Sea over the last 15,000 years. Org. Geochem. 34, 1057–1070.
Müller, Peter J., Fischer, Gerhard, 2004. C_{37}-Alkenones as paleotemperature tool: fundamentals based on sediment traps and surface sediments from the south Atlantic ocean. In: Wefer, G., Mulitza, S., Ratmeyer, V. (Eds.), The South Atlantic in the Late Quaternary: Reconstruction of Material Budgets and Current Systems. Springer, Berlin, Heidelberg, New York, pp. 167–193.
Müller, P.J., Kirst, G., Ruhland, G., Von Storch, I., Rosell-Melé, A., 1998. Calibration of the alkenone paleotemperature index $U^{K'}_{37}$U 37 K′ based on core-tops from the eastern South Atlantic and the global ocean (60° N-60° S). Geochem. Cosmochim. Acta 62, 1757–1772.
Müller, J., Werner, K., Stein, R., Fahl, K., Moros, M., Jansen, E., 2012. Holocene cooling culminates in sea ice oscillations in Fram Strait. Quat. Sci. Rev. 47, 1–14.
Nilsen, F., Cottier, F., Skogseth, R., Mattsson, S., 2008. Fjord–shelf exchanges controlled by ice and brine production: the interannual variation of Atlantic Water in Isfjorden, Svalbard. Cont. Shelf Res. 28, 1838–1853.
Onarheim, I.H., Eldevik, T., Årthun, M., Ingvaldsen, R.B., Smedsrud, L.H., 2015. Skillful prediction of Barents Sea ice cover. Geophys. Res. Lett. 42, 5364–5371.
Oziel, L., Sirven, J., Gascard, J.-C., 2016. The Barents Sea frontal zones and water masses variability (1980–2011). Ocean Sci. 12, 169–184.
Oziel, L., Neukermans, G., Ardyna, M., Lancelot, C., Tison, J.L., Wassmann, P., Sirven, J., Ruiz-Pino, D., Gascard, J.C., 2017. Role for Atlantic inflows and sea ice loss on shifting phytoplankton blooms in the Barents Sea. J. Geophys. Res.: Oceans 122, 5121–5139.
Pathirana, I., Knies, J., Felix, M., Mann, U., 2014. Towards an improved organic carbon budget for the western Barents Sea shelf. Clim. Past 10, 569–587.
Pearce, C., Seidenkrantz, M.-S., Kuijpers, A., Massé, G., Reynisson, N.F., Kristiansen, S.M., 2013. Ocean lead at the termination of the Younger Dryas cold spell. Nat. Commun. 4, 1664.
Pfirman, S., Bauch, D., Gammelsrød, T., 1994. The Northern Barents Sea: Water Mass Distribution and Modification. AGU, American Geophysical Union.
Piwosz, K., Walkusz, W., Hapter, R., Wieczorek, P., Hop, H., Wiktor, J., 2009. Comparison of productivity and phytoplankton in a warm (Kongsfjorden) and a cold (Hornsund) Spitsbergen fjord in mid-summer 2002. Polar Biol. 32, 549–559.
Polyak, L., Alley, R.B., Andrews, J.T., Brigham-Grette, J., Cronin, T.M., Darby, D.A., Dyke, A.S., Fitzpatrick, J.J., Funder, S., Holland, M., 2010. History of sea ice in the Arctic. Quat. Sci. Rev. 29, 1757–1778.
Polyakov, I.V., Pnyushkov, A.V., Alkire, M.B., Ashik, I.M., Baumann, T.M., Carmack, E.C., Goszczko, I., Guthrie, J., Ivanov, V.V., Kanzow, T., 2017. Greater role for Atlantic inflows on sea-ice loss in the Eurasian basin of the Arctic ocean. Science 356 (6335), 285–291.
Rasmussen, T.L., Thomsen, E., 2014. Brine formation in relation to climate changes and ice retreat during the last 15,000 years in Storfjorden, Svalbard, 76–78° N. Paleoceanography 29, 911–929.
Rasmussen, T.L., Thomsen, E., Ślubowska, M.A., Jessen, S., Solheim, A., Koç, N., 2007. Paleoceanographic evolution of the SW Svalbard margin (76° N) since 20,000 14C yr BP. Quat. Res. 67, 100–114.
Rasmussen, T.L., Thomsen, E., Nielsen, T., Wastegård, S., 2011. Atlantic surface water inflow to the Nordic seas during the Pleistocene–Holocene transition (mid–late Younger Dryas and Pre-Boreal periods, 12 450–10 000 a BP). J. Quat. Sci. 26, 723–733.
Rasmussen, T.L., Thomsen, E., Skirbekk, K., Ślubowska-Woldengen, M., Kristensen, D.K., Koç, N., 2014. Spatial and temporal distribution of Holocene temperature maxima in the northern Nordic seas: interplay of Atlantic-, Arctic- and polar water masses. Quat. Sci. Rev. 92, 280–291.
Reimer, P.J., Bard, E., Bayliss, A., Beck, J.W., Blackwell, P.G., Bronk Ramsey, C., Buck, C.E., Cheng, H., Edwards, R.L., Friedrich, M., Grootes, P.M., Guilderson, T.P., Haflidason, H., Hajdas, I., HattÃ, Š.C., Heaton, T.J., Hogg, A.G., Hughen, K.A., Kaiser, K.F., Kromer, B., Manning, S.W., Niu, M., Reimer, R.W., Richards, D.A., Scott, E.M., Southon, J.R., Turney, C.S.M., van der Plicht, J., 2013. IntCal13 and MARINE13 radiocarbon age calibration curves 0–50,000 years cal BP. Radiocarbon 55, 1869–1887.
Risebrobakken, B., Berben, S.M.P., 2018. Early Holocene establishment of the Barents Sea Arctic front. Front. Earth Sci. 6, 166.
Risebrobakken, B., Moros, M., Ivanova, E.V., Chistyakova, N., Rosenberg, R., 2010. Climate and oceanographic variability in the SW Barents Sea during the Holocene. Holocene 20 (4), 609–621.
Risebrobakken, B., Dokken, T., Smedsrud, L.H., Andersson, C., Jansen, E., Moros, M., Ivanova, E.V., 2011. Early Holocene temperature variability in the Nordic Seas: the role of oceanic heat advection versus changes in orbital forcing. Paleoceanography 26, PA4206.
Ritz, S.P., Stocker, T.F., Grimalt, J.O., Menviel, L., Timmermann, A., 2013. Estimated strength of the Atlantic overturning circulation during the last deglaciation. Nat. Geosci. 6, 208–212.
Rosell-Melé, A., 1998. Interhemispheric appraisal of the value of alkenone indices as temperature and salinity proxies in high-latitude locations. Paleoceanography 13 (6), 694–703.
Rosell-Melé, A., Carter, J., Eglinton, G., 1994. Distributions of long-chain alkenones and alkyl alkenoates in marine surface sediments from the North East Atlantic. Org. Geochem. 22, 501–509.
Rosell-Mele, A., Weinelt, M., Sarnthein, M., Koc, N., Jansen, E., 1998. Variability of the Arctic front during the last climatic cycle: application of a novel molecular proxy. Terra Nova Oxford 10, 86–89.
Rudels, B., Korhonen, M., Schauer, U., Pisarev, S., Rabe, B., Wisotzki, A., 2015. Circulation and transformation of Atlantic water in the Eurasian basin and the contribution of the Fram Strait inflow branch to the Arctic ocean heat budget. Prog. Oceanogr. 132, 128–152.
Rueda, G., 2013. Reconstructing Climate Variability in the North Atlantic during the Late Holocene: an Integrated Biomarker Approach the Autonomous University of Barcelona. The Autonomous University of Barcelona, Barcelona, p. 179.
Salvigsen, O., 2002. Radiocarbon-dated *Mytilus edulis* and *Modiolus modiolus* from northern Svalbard: climatic implications. Norsk Geografisk Tidsskrift-Norwegian J. Geog. 56, 56–61.
Schauer, U., Rudels, B., Fer, I., Haugan, P., Skogseth, R., Björk, G., Winsor, P., 2003. Return of Deep Shelf/Slope Convection in the Western Barents Sea, Seventh Conference on Polar Meteorology and oceanography and Joint Symposium on High-Latitude Climate Variations. The American Meteorological Society.
Serreze, M.C., Barry, R.G., 2011. Processes and impacts of Arctic amplification: a research synthesis. Glob. Planet. Chang. 77, 85–96.
Skogseth, R., Haugan, P., Haarpaintner, J., 2004. Ice and brine production in Storfjorden from four winters of satellite and in situ observations and modeling. J. Geophys. Res.: Oceans 109, C10008.
Slagstad, D., Ellingsen, I., Wassmann, P., 2011. Evaluating primary and secondary production in an Arctic Ocean void of summer sea ice: an experimental simulation approach. Prog. Oceanogr. 90, 117–131.
Ślubowska, M.A., Koç, N., Rasmussen, T.L., Klitgaard-Kristensen, D., 2005. Changes in the flow of Atlantic water into the Arctic Ocean since the last deglaciation: evidence from the northern Svalbard continental margin, 80°. N. Paleoceanogr. 20 (4), PA4014.
Ślubowska-Woldengen, M., Koç, N., Rasmussen, T.L., Klitgaard-Kristensen, D., Hald, M., Jennings, A.E., 2008. Time-slice reconstructions of ocean circulation changes on the continental shelf in the Nordic and Barents Seas during the last 16,000 cal yr BP. Quat. Sci. Rev. 27, 1476–1492.
Smedsrud, L.H., Esau, I., Ingvaldsen, R.B., Eldevik, T., Haugan, P.M., Li, C., Lien, V.S., Olsen, A., Omar, A.M., Otterå, O.H., 2013. The role of the Barents Sea in the Arctic climate system. Rev. Geophys. 51, 415–449.
Smith, W.O., Sakshaug, E., 1990. Polar phytoplankton. In: Smith, W.O. (Ed.), Polar Oceanography, Part B: Chemistry, Biology and Geology. Academic Press, New York, pp. 447–525.
Stuiver, M., Reimer, P.J., 1993. Extended 14C database and revised CALIB radiocarbon calibration program. Radiocarbon 35, 215–230.
Thorarinsdóttir, G.G., Gunnarsson, K., 2003. Reproductive cycles of *Mytilus edulis* L. on the west and east coasts of Iceland. Polar Res. 22, 217–223.
Trudnowska, E., Gluchowska, M., Beszczynska-Möller, A., Blachowiak-Samolyk, K., Kwasniewski, S., 2016. Plankton patchiness in the polar front region of the west Spitsbergen shelf. Mar. Ecol. Prog. Ser. 560, 1–18.
Volkman, J.K., Eglinton, G., Corner, E.D., Forsberg, T., 1980. Long-chain alkenes and alkenones in the marine coccolithophorid *Emiliania huxleyi*. Phytochem 19, 2619–2622.
Walczowski, W., 2013. Frontal structures in the west Spitsbergen current margins. Ocean Sci. 9 (6), 957–975.
Wollenburg, J.E., Knies, J., Mackensen, A., 2004. High-resolution paleoproductivity fluctuations during the past 24 kyr as indicated by benthic foraminifera in the marginal Arctic Ocean. Palaeogeogr. Palaeoclimatol. Palaeoecol. 204, 209–238.
Yang, X.-Y., Yuan, X., Ting, M., 2016. Dynamical link between the Barents–Kara Sea Ice and the Arctic oscillation. J. Clim. 29, 5103–5122.
Zajączkowski, M., 2008. Sediment supply and fluxes in glacial and outwash fjords, Kongsfjorden and Adventfjorden. Svalbard. Polish Polar Res. 29, 59–72.
Zajączkowski, M., Nygård, H., Hegseth, E.N., Berge, J., 2010. Vertical flux of particulate matter in an Arctic fjord: the case of lack of the sea-ice cover in Adventfjorden 2006–2007. Polar Biol. 33 (2), 223–239.
Łącka, M., Pawłowska, J., Zajączkowski, M., 2015a. New Methods in the Reconstruction of Arctic Marine Palaeoenvironments, Impact of Climate Changes on Marine Environments. Springer, pp. 127–148.
Łącka, M., Zajączkowski, M., Forwick, M., Szczuciński, W., 2015b. Late Weichselian and Holocene palaeoceanography of Storfjordrenna, southern Svalbard. Clim. Past 11, 587–603.